Influence of slow or fast surface traps on the amplitude and symmetry of the piezoelectric response of semiconducting-nanowire-based transducers

Andrés Jenaro Lopez Garcia, Mireille Mouis, Alessandro Cresti, Ran Tao, Gustavo Ardila

Author version. Original paper reference: Journal of Physics D: Applied Physics, Vol. 55, no. 405502, 13pp, doi:10.1088/1361-6463/ac8251 (Aug. 2022). HAL reference: hal-03763834

Influence of slow or fast surface traps on the amplitude and symmetry of the piezoelectric response of semiconducting-nanowire-based transducers

Authors:

Andrés Jenaro Lopez Garcia, Mireille Mouis, Alessandro Cresti, Ran Tao[1], Gustavo Ardila

Univ. Grenoble Alpes, CNRS, Grenoble INP, IMEP-LaHC, F-38000 Grenoble, FRANCE

E-mail: mouis@minatec.grenoble-inp.fr, ardilarg@minatec.grenoble-inp.fr

Keywords: traps dynamics, finite element method, piezoelectric sensor, mechanical energy harvesting, ZnO, nanogenerator, surface Fermi level pinning

Abstract:

ZnO nanowires are excellent candidates for energy harvesters, mechanical sensors, piezotronic and piezophototronic devices. These nanowires are usually non-intentionally n-doped during their growth. The essential role of doping, surface traps and surface Fermi level pinning in the actual response of piezoelectric semiconductors has already been demonstrated. In order to go further, this paper investigates the influence of the density and of the dynamics of surface traps on such important parameters as the output generated potential and the effective piezoelectric coefficient. We implemented numerical simulations based on the finite element method combining the mechanical, piezoelectric, and semiconducting characteristic of ZnO nanowires array based nanocomposites (the so-called VING configuration) operated in compression. It was found that a certain amount of surface traps was required to obtain a usable generated output potential from the studied devices in the range of dimensions and doping level reported in most experimental results. Moreover, the surface traps influence was strongly dependent on their dynamics. As a

[1] Present address : Key Laboratory of Optoelectronic Devices and Systems of Ministry of Education and Guangdong Province, College of Physics and Optoelectronic Engineering, Shenzhen University, Shenzhen 518060, CHINA

first step towards the analysis of traps dynamics, we compared the two extreme cases of ultra-slow and ultra-fast traps. The symmetry and asymmetry of the piezoelectric response and a comparison to thin film was also discussed. This study demonstrates that the realistic modelling of the piezoelectric response of semiconductor based transducers should account for traps dynamics effects.

1. Introduction

Piezoelectric Nanowires (NWs) are very promising structures thanks to their piezoelectric properties and their semiconducting nature. These properties have been studied for many applications ranging from sensors [1] to energy harvesters [2], and in new fields like piezotronics [3] and piezophototronics [4]. In particular, ZnO semiconducting NWs present excellent piezoelectric properties and can be fabricated at low temperatures, which makes them compatible with many types of substrates, including flexible ones, and with above integrated circuit (above-IC) silicon integration [5–7]. Numerous theoretical and experimental studies have been performed on individual ZnO NWs and on devices integrating these NWs, such as nanocomposites, where vertical NWs are grown from a seed layer and immerged in a dielectric matrix. This is the so-called Vertically Integrated Nanogenerator structure (VING) [8,9].

Experimentally, VINGs show quite high piezoelectric responses under compressive or bending forces. In this paper, the piezoelectric response is defined as the output potential generated in open circuit conditions, as a result of a change in the input mechanical load. There have been several experimental demonstrations in the literature of ZnO based VING performance. For instance, a VING device integrating 4μm long and 400nm wide ZnO NWs in a polymer matrix (PMMA) produced about 150mV under compression [10]. In ref. [11], the authors reported similar results (about 100mV generated) when a compressive force of 1.5N (corresponding to a pressure of 15kPa) was applied on VING devices integrating 3μm long and 300nm wide ZnO NWs. Hu et al. [12] reported output potentials of several volts from similar VING structures integrated on both sides of a polyester film under an applied strain of 0.12%. Zhu et al. [13] showed that small VINGs connected in parallel could produce a voltage of 35V under a compression of 1MPa. All these examples show that ZnO NWs are able to provide an efficient

piezoelectric response. However, such good results are by no means obvious. Indeed, ZnO is usually non intentionally doped, so that the piezoelectric effect is potentially screened by ionized dopants and free charges [14].

The influence of doping and free carrier screening on the piezoelectric response of semiconducting (mostly ZnO) nanowires has been studied theoretically by means of simulation. Even under the assumption of full depletion, a large doping concentration results in degraded performance, as demonstrated for a VING device under compression [15]. The presence of free charges in the core of the nanowire raises even stronger issues, as they can screen the strain-induced piezoelectric potential. This has been explored by simulation. In ref. [16], the equilibrium potential resulting from the coupling of piezoelectric and semiconducting equations was calculated by the Finite Element Model (FEM) method in the case of individual ZnO NWs of given diameter (300nm) and length (4µm), and variable doping concentration. It was shown that the piezoelectric potential under axial compression is actually independent of nanowire length once this length is larger than depletion depth, and that it is smaller at larger doping concentrations. This limitation was the result of the polarisation field screening by free carriers, except in a depleted region of limited extension at the top of the nanowire. A theoretical maximum of about 10 mV was obtained for an axial compression of 6.25 MPa with a doping concentration N_d of 10^{17} cm^{-3}. Later, Fathi et al. [17] simulated a 50nm wide and 600nm long ZnO NW under a compressive force of 80nN (corresponding to a pressure of 41MPa). The authors initially considered very low doping concentrations ranging from 10^9 cm^{-3} up to 10^{12} cm^{-3}. They concluded as well that the application of the force produces a depletion region only at the top of the nanowire, where the piezoelectric potential (open-circuit) is generated, and that an increase of doping concentration reduces the piezoelectric response. In a second set of simulations, they added an external surface charge density, ranging from -0.002 $C.m^{-2}$ to -0.08 $C.m^{-2}$, at the top of the NW in order to extend the depleted region. The piezoelectric response was increased, until an eventual saturation, as in ref. [18]. For a doping concentration of $10^{11}cm^{-3}$, the potential was found to saturate at 250mV for external surface charge values beyond -0.03 $C.m^{-2}$.

In contrast to these theoretical predictions, several experiments have shown that a variation of ZnO NWs length does influence the piezoelectric response. For instance, in ref. [7], vertical ZnO NWs with different lengths were deflected by the scanning of a conducting AFM (Pt/Si) tip over the sample. The longer NWs (3-5µm long and 100-200nm wide) were grown by Vapor Liquid Solid (VLS) on a SiC substrate, while the shorter ones (1-2µm long and 200nm wide) were grown by Aqueous Chemical Growth (ACG) both on SiC and Si substrates. The longer NWs generated on average 30-35mV, while the shorter ones generated about 5mV. The authors ruled out the role of the substrate. However, they could not discriminate between the roles of geometry and of growth-dependent doping level. In ref. [19], ZnO NWs of different lengths (from 1.3µm to 4.7µm) fabricated by Chemical Bath Deposition (CBD) were integrated into VING devices and characterized under a compressive force of 0.5N. The electrical energy generated by the devices with longer NWs was about 4 times larger (35nJ) than with shorter NWs.

There have also been some experimental results about the role of doping concentration on VING devices performance, although with GaN, which allows an easier doping level control than ZnO. In ref. [14], VING devices integrating 100nm wide and 500nm long GaN NWs with different doping concentrations (from 10^{17}cm^{-3} to 10^{19}cm^{-3}) were characterized under compression (1MPa). Their output voltage dropped when the doping concentration increased, which is consistent with the simulations of Romano et al. [16]. The maximum generated output voltage was about 80mV for the lowest doping concentration (7.58×10^{17}cm^{-3}), which is quite low compared to previously mentioned experimental results [12,13].

In order to explain the large piezo-response obtained in VING experiments in spite of nanowire doping, it is necessary to assume that nanowires are fully depleted from free carriers on their whole length. This can be obtained with a density of charge along the surface of the nanowire, whatever its origin. Its effect has been quantified, for instance by Kim et al. [18], who simulated a 100nm wide and 600nm long ZnO NW, with donor concentration $N_d = 10^{17} cm^{-3}$, surrounded by a negative surface charge density up to -0.02 C.m^{-2}, under 10MPa axial compression. The generated piezoelectric potential (open-circuit) actually increased as the NW was depleted from its free charges under the electrostatic influence of the external surface charge. However, the piezoelectric potential saturated at 650mV for surface charges beyond -0.01 C.m^{-2}.

An earlier paper explored the role of the surface charge associated with the presence of interface states in ZnO VING devices [20]. Indeed, at the surface of III-V and II-VI semiconductor materials like GaN [21–25] and ZnO [26–29], or at their interface with other materials, the Fermi level is usually not free and can even be pinned in the bandgap. Fermi level pinning and consequent surface band bending result from the presence of interface states in the bandgap, which act as electron and hole traps. In the case of n-doped ZnO, acceptor-like surface states (related to chemisorbed oxygen, hydrogen or hydroxyl groups) are occupied by electrons, thus inducing upward band bending and electron depletion at the NW surface [30]. The relation between the position of the surface Fermi level (SFL) and the density of interface states is recalled in the Supporting Information of ref. [20] in the case of a uniform distribution of states in the bandgap. The presence of surface states and surface band bending in ZnO NWs has been evidenced in several experiments. Soudi et al. [30] used Kelvin Probe Force Microscopy (KPFM) to determine surface barrier height through surface photovoltage in ZnO NWs with different diameters. Under low-level optical excitations, they detected a decrease of the work function of the NW surface, which indicates a lowering of the initial upward surface band bending. With the help of FEM electrostatic simulations, they calculated the density of surface states, which increased for diameters below 40nm. Al-Saadi et al. [31] treated 120nm wide and 3.5µm long ZnO NWs with atomic hydrogen in the presence or in the absence of H_2O. They used X-ray Photoemision Spectroscopy (XPS) and Ultraviolet Photoemission Spectroscopy (UPS) to measure the band bending at the surface of the NW. They found an upward band bending consistent with the creation of surface defects in the absence of H_2O and a downward bending in the presence of H_2O, which led to electron depletion and accumulation at the surface, respectively.

Although acknowledged in III-V materials, Fermi level pinning and the presence of surface and interface traps have seldom been accounted for in simulations, when dealing with piezoelectric nanocomposites and sensors. Yet, we believe that they play an essential role in the actual response of piezoelectric semiconductors. Indeed, for $N_d = 10^{17} cm^{-3}$ (typical on grown ZnO NWs) and low surface-trap density N_{it}, there is no surface band bending. This is known as the free SFL assumption, which is the usual assumption in most simulations, although it is quite unlikely. In this case, because of the screening by free carriers, the application of a pressure to the

VING generates a polarization field that depletes only the top of the NWs [16,17,20,32], while the rest of the nanowire remains neutral, with no contribution of the polarization field to the generated potential. In contrast, in the presence of traps along the surface of the nanowire, energy bands will bend near the surface and potentially deplete the nanowire laterally, from its sidewalls. If the surface trap density is large enough, it becomes possible to deplete the NW until its core, and the whole volume can contribute to the generated piezoelectric potential [20]. Moreover, it should be noted that, due to the inverse piezoelectric effect, a large surface trap density can strain the ZnO NW and induce polarization even in the absence of an external mechanical load.

Recently, there has been a first attempt to account for surface traps in VING simulations [20]. The devices integrated ZnO NWs (with typical dimensions of 100nm in diameter and 600nm in length) surrounded by a polymer matrix of PMMA. They have been simulated by FEM both in compressive and bending modes. Different doping concentrations have been considered, ranging from $10^{16}cm^{-3}$ up to $10^{18}cm^{-3}$. In addition to the local-voltage dependent free carrier concentration, a surface charge has been introduced either on the NW top or on the entire NW surface, at the interface between ZnO and PMMA. This surface charge was a function of the surface traps density N_{it} and of the local potential. A moderate density of surface traps ($5\times10^{11}cm^{-2}eV^{-1}$) on the entire NW surface was sufficient to fully deplete the nanowire for doping levels up to about $10^{17}cm^{-3}$. Under these conditions, the piezo-response to an axial compression became length dependent and could start to reach values of practical interest, consistently with above-mentioned experiments [7,19]. However, it is important to remember that, in these simulations, surface traps have been considered as ultra-slow, i.e., it has been assumed that they did not have the time to charge or discharge within the time frame of the piezoelectric response induced by a change in the mechanical load.

In the present paper, we will evaluate the limits of this assumption. Indeed, the dynamics of surface traps can be affected by several parameters. For instance, for surface traps arising from local states in the dielectric material (PMMA in our case) situated in the close vicinity of nanowire surface, the trap response will be all the faster as the local state is closer to the interface. It would go beyond the scope of this paper to provide an exact description of the energy and space distribution of the states that can act as traps at the ZnO/PMMA interface. The aim here is rather to highlight general trends so that we focused on the two extreme cases of ultra-slow traps,

which remain in their initial state and are not affected by mechanical actuation, and ultra-fast traps, for which a permanent thermodynamic equilibrium is maintained at all interfaces at all time.

We will also investigate the piezoelectric parameters (especially d_{33} in the case of a uniaxial compression) that are useful to evaluate the piezoelectric performance in the linear regime.

Most experimental reports on the measurement of the piezoelectric coefficients of ZnO NWs have focused on the determination of the effective value of d_{33} (noted d_{33}^{eff} in the following). Experimentally, d_{33}^{eff} is deduced from the deformation along the c-axis that results from a voltage difference along the same direction. It is related to the d_{33} coefficient of the piezoelectric tensor of the material but, due to the nanowire topology, it usually depends as well on the d_{31} shear coefficient. Measurements have been performed either by nanoindentation or by Piezoelectric Force Microscopy (PFM). Tamvakos et al. [33] performed PFM measurements (AFM tip with stiffness of 8.8N/m and compressive force of 80nN at 40kHz) on 150nm wide and 1.5µm long ZnO NWs fabricated by Electrochemical Deposition (ECD) on Si/Au substrates and obtained a d_{33}^{eff} value of 11.8pm/V. Brotman et al. [34] used nanoindentation (compressive force in the range of 0.2mN-6mN) on 150nm wide and 2.3µm long ZnO NWs grown by ACG on a paper/PEDOT:PSS substrate, and obtained a d_{33}^{eff} value of 9.2pm/V. Fan et al. [35] used PFM (AFM tip with a stiffness of 3N/m with a compressive force of 150nN at 33kHz) on 300nm wide and 2µm long ZnO NWs grown by Vapor Diffusion Deposition on GaN substrates, and extracted a d_{33}^{eff} value of 7.5pm/V. Scrymgeour et al. [36] performed PFM (AFM tips with stiffness of 14N/m and 40N/m operated at 15kHz) on 150nm wide and 600nm long ZnO NWs grown by CBD on Ag films, and measured a d_{33}^{eff} of 4.41pm/V. It is worth mentioning that Cavallini et al. [37] characterized 30nm wide ZnO NWs grown by the same CBD method on glass/ITO and PET/ITO substrates using PFM as well (AFM tip with a stiffness of 5N/m operated at 15kHz), and obtained 2.13pm/V for d_{33}^{eff} on rigid substrate, and 5.2pm/V on flexible substrate. Quang et al. [38] in particular explored the piezoelectric response of NWs and thin films fabricated by MOCVD. They found that the response was higher with NWs (d_{33}^{eff} = 4.36pm/V) than with thin films (d_{33}^{eff} = 2.5pm/V). Thus, the d_{33}^{eff} values obtained experimentally on nanowires are ranging from 2 pm/V to 12 pm/V, to be compared with the d_{33}^{eff} value of bulk ZnO (9.93pm/V) [39] and

of ZnO thin films (in the range of 2.5 to 8 pm/V) [38,40–42]. However, the results may be affected by measurement conditions, such as the use of low stiffness AFM tips, which can lead to topographical artefacts [36] and larger electrostatic perturbing effects [38,43,44]. Substrate and electrode materials can as well affect the electromechanical response [45]. The fabrication method could also lead to differences in doping concentrations, defects and surfaces states [31], thus making the comparison between different experiments difficult.

The literature provides very few theoretical models for the calculation of the piezoelectric coefficients of ZnO NWs. Kim et al. [46] performed FEM simulations based on standard piezoelectric equations of cylindrical ZnO structures. They considered NWs with diameters between $100nm$ and $500nm$ and large disks with diameters between $700nm$ and $5\mu m$. A vertical compressive pressure of 10 MPa was applied on top of the structures. The calculated d_{33}^{eff}, obtained with a conventional theoretical approach[2], varied along the z-axis and was as a function of the diameter. Overall, thinner structures featured larger d_{33}^{eff} ($\sim 10.5\, pC/N$) than wider structures (below ~8.5 pC/N). This effect was explained by a reduction of radial stress in thinner structures. Hoang et al. [47] developed a continuum model of piezoelectric NWs that combined bulk and surface terms, both extracted from first-principle calculations, where surface terms accounted for the atomistic rearrangement of surface atoms with respect to bulk. The corresponding equations were then solved by FEM. They found that d_{33}^{eff} increases as diameter decreases, but only for diameters below 6nm. For larger diameters, the coefficient approached that of bulk. However, none of these simulations did account for the influence of free carriers, the presence of neutral regions and other semiconducting effects, which can influence experimental d_{33}^{eff} values exactly by the same mechanisms as they influence piezoelectric response, and may explain part of the dispersion in experimental values. Moreover, there has been no theoretical evaluation of d_{33}^{eff} for the configuration used in VING devices.

In this work, we theoretically explored the role of free carriers and surface traps on the output potential and on the effective piezoelectric coefficient d_{33}^{eff} of piezoelectric nanocomposites based on ZnO NWs in VING configuration. The performance of these nanocomposites is

[2] A function that depends on the piezoelectric coefficients d_{33} and d_{31}, the elastic compliance and the stress along the *x* or *y* axis. This function was deduced under the assumption of a constant electric field.

compared to that of thin films. As a first step towards the analysis of traps dynamics, we compared the two extreme cases of ultra-slow and ultra-fast traps. The study was performed by solving the full set of coupled equations that describe the mechanical, piezoelectric and semiconducting properties of the structure, within a FEM approach. The devices were operated in compression, as in most experimental reports, but our conclusions are general.

2. Device under study

For this study, we used a classical VING structure configuration. Figure 1 shows a typical implementation on a stainless steel foil substrate, which provides the bottom contact. A silicon substrate can be used as well.

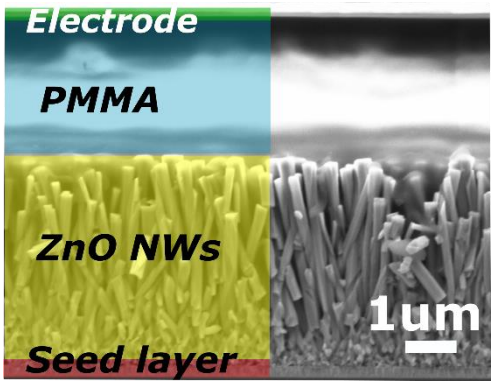

Fig 1. SEM image of a typical VING device based on ZnO NWs grown on Si substrate by using Chemical Bath Deposition (CBD).

The active layer consists of an array of vertical n-type ZnO NWs immerged in a dielectric matrix which provides mechanical robustness (yellow region). A thin ZnO seed layer (in red) is deposited on the substrate to promote NW growth. The active layer is separated from top contact (in green) by a dielectric layer (in blue), usually obtained by increasing the amount of matrix material so that it caps the array of ZnO NWs.

Experimentally, the ZnO NWs integrated in this kind of device feature diameters between 150 nm and 300 nm and lengths between 1 µm and 5 µm [9,10,41], while the typical n-type doping is in the range from 10^{17}cm^{-3} to 10^{18}cm^{-3} [14]. Theoretical studies have usually assumed

doping concentrations in the range from 10^{15}cm^{-3} to 10^{18}cm^{-3} [16,17,20,49–53] with typical 200 nm wide and 600 nm to 3 µm long NWs [54–56]. Concerning the other geometrical parameters, experimental works have reported thicknesses in the range from 50 nm to 200 nm for the seed layer, and from 0.6 µm to 2 µm for the dielectric cap layer above the NWs [11–13,57] , while simulations have used 50 nm thick seed layers and 100 nm thick insulating cap layers [20]. In this work, the considered geometry featured 100 nm wide and 3 µm long ZnO NWs, a 40 nm thick seed layer, a 1 µm thick insulating cap layer, and PMMA as matrix and cap layer material. The varied parameters were the doping level and, as discussed below, the surface traps characteristics at the interface between ZnO and PMMA.

2.1 Device operation and role of traps

The VING device operates in capacitive mode. We will concentrate on device operation in compression, with a rigid substrate (Fig. 2).

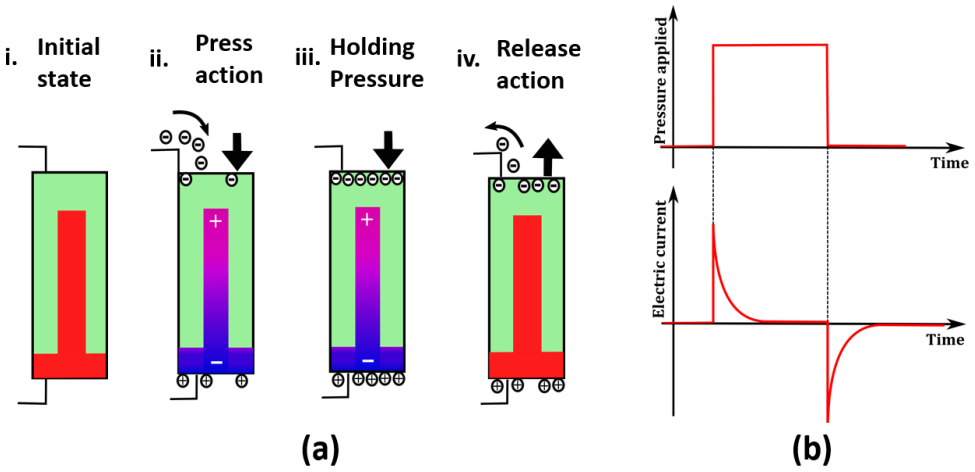

Fig. 2. (a) Schematic operation of a VING unit cell connected to an external resistive load. It consists of 4 steps: i) initial state, ii) "Press": a force is applied on top surface, creating a polarization inside the NW, iii) "Hold": the force is maintained long enough to allow equilibrium to be reached, iv) "Release": the force is withdrawn. **(b)** Schematic representation of the electric current pulses generated during these successive steps as a function of time.

In practical applications, the device is electrically loaded. When a mechanical load is applied on the top ("Press" action), the NWs are deformed, a strain field is produced in ZnO, and dipoles are

generated by local deformation of crystal mesh, thus creating a polarization field that induces a charge on the two electrodes. A transient current flows in the external circuit until the polarization charge is screened. When the mechanical load is released ("Release" action), the opposite phenomena occur, with current flowing in the opposite direction. For practical use in energy harvesters, the generated voltage and current pulses are often rectified before the electrical energy is stored into a capacitor or other storage devices [58,59].

We will focus on "Press" action, where the device has no external mechanical load in its initial state and is subjected to a vertical mechanical compression in the final state, and "Release" action, which corresponds to the reverse process. From a theoretical point of view, the "Press" and "Release" actions result in a variation of the potential difference between the electrodes. This variation is a direct consequence of the variation of strain-induced polarization and can be affected by the presence of free carriers in the NW or by surface traps charges.

3. Simulation framework

In this work, we used a Finite Element Modelling (FEM) approach to simulate the full set of differential equations that couple mechanical, piezoelectric and semiconducting properties. Concerning the dynamics of surface traps at the ZnO/PMMA interface, two extreme cases were considered : ultra-fast and ultra-slow traps. The assumptions underlying the "ultra-fast traps" case was that the thermodynamic equilibrium of surface traps charge was reached instantaneously so that the density of traps could be written as a function of the local potential obtained *after* the "Press" or "Release" action. In contrast, in the case of "ultra-slow traps", the traps were assumed to retain their initial equilibrium electric charges so that their density could be written as a function of the local potential obtained *before* the "Press" or "Release" actions. Moreover, we evaluated the piezoelectric coefficient using COMSOL Multiphysics environment to run time-dependent simulations of the electrically loaded VING structure.

3.1. Simulated structure

Performing simulations that involve the coupling of piezoelectric and semiconductor physics on a whole VING structure, which can include billions of NWs, would be much too expensive in computer resources. In order to reduce computational cost, we adopted a convenient strategy which consists in reducing the simulation space to a single unit cell of the device, here made up of a single ZnO NW surrounded by an insulating (PMMA) matrix over a ZnO seed layer. A 2D axisymmetric cylindrical model was used for the unit cell, as shown in Fig. 3. This further reduces computing cost while keeping a fair image of the normally hexagonal geometry. The 3D geometry was obtained by the rotation of the 2D profile around the NW axis, as shown in Fig. 3 (a). To validate the VING model, we carried out as well the simulation of a thin film cell with almost the same dimesions as the VING structure, as shown in Fig. 3 (c). With this approach, all equations and parameters must be transformed from Cartesian to cylindrical, vertical (z) and radial (r), coordinates.

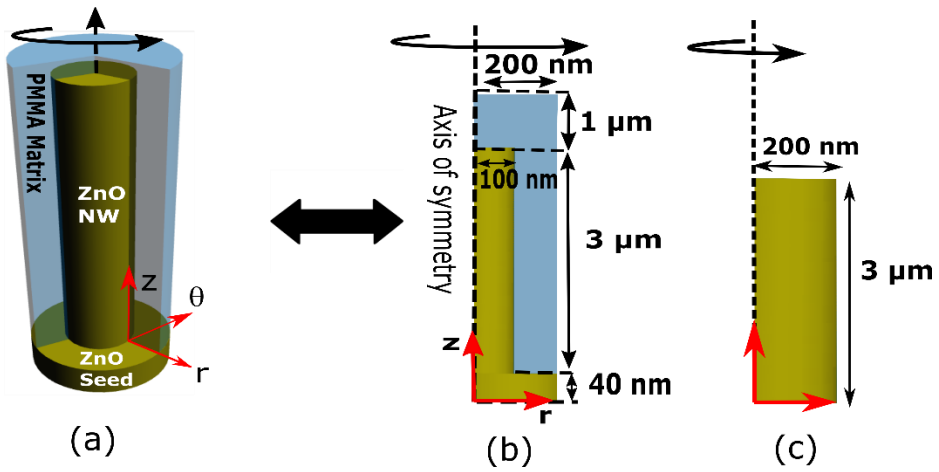

Fig. 3. Schematic of a single unit cell of : (a) A cylindrical geometry of the VING device. (b) 2D axisymmetric VING model considered in the simulation. (c) 2D axisymmetric ZnO thin film cell.

3.2. Coupled system of mechanical/electrical equations

In order to evaluate the piezoresponse of a given structure under external pressure variation, we calculated the variation of inter-electrode potential between the final and initial states, before and after the variation of mechanical load, respectively (see more details in the supporting information, Figures S1, S2 and Table S1). We considered the following set of equations, which relate mechanical and electrical properties of a piezoelectric material:

$$[\sigma(t)] = [c][\varepsilon(t)] - [e]^T[E(t)] \,, \quad (1)$$

$$[D(t)] = [e][\varepsilon(t)] + [\kappa][E(t)] \,, \quad (2)$$

where $[\sigma]$ is the stress matrix, $[\varepsilon]$ is the strain matrix, $[E]$ is the electric field vector, $[D]$ is the electric displacement vector, $[c]$ is the elasticity matrix, $[\kappa]$ is the dielectric constant matrix and $[e]$ is the piezoelectric coefficient matrix. The coupling between piezoelectric and semiconductor physics is introduced by the two matrices $[e]$ and $[e]^T$, which correspond to the direct and inverse piezoelectric effects, respectively.

In addition to these equations, mechanical and electrical equilibrium conditions must be fulfilled. Electrical equilibrium is described by Poisson's equation:

$$\nabla \cdot D(t) = \rho(t) \,, \quad (3)$$

where ρ is the local density of charge. In the semiconducting regions, we have

$$\rho(t) = q(p(t) - n(t) + N_d^+ - N_A^-) \,, \quad (4)$$

where n and p are the density of electrons and holes, respectively, and N_A^- and N_d^+ are the density of acceptor and donor atoms, respectively. In our case, the active material is ZnO, which was considered as an n-type semiconductor where N_A^- is negligible. Volume traps were neglected. Electron and hole concentrations are function of the local electric potential. We used the Boltzmann statistics to describe the free carrier concentrations below degeneracy (around 10^{18} cm^{-3} in ZnO). Dielectric regions were supposed free of charges, i.e.

$$\rho = 0 \quad (5)$$

Transient mechanical behaviour was described using Cauchy momentum equation given by

$$f_v(\mathrm{t}) + \rho_m^{-1}(\nabla \cdot \sigma(\mathrm{t})) = \frac{d^2u}{dt^2}\,, \tag{6}$$

where ρ_m, u, and *t* are the local mass density (*per* unit of volume), the displacement vector (*r* and *z* displacements) and time. We assumed that there was no body force (f_v) on the VING model ($f_v = 0$) and used equations (1) and (2) for mechanical and electrical conditions. We obtained the following system of differential equations, which couples local strain [ε] with local electric potential *V*:

$$\nabla([c][\varepsilon(t)]) + \nabla\left([e]^T\vec{\nabla}V(t)\right) = \rho_m\frac{d^2u}{dt^2}\ , \tag{7}$$

$$\nabla\left([\kappa]\vec{\nabla}V(t)\right) - \nabla([e][\varepsilon(t)]) = \rho(t)\ . \tag{8}$$

With the appropriate boundary conditions, these equations provide the output potential of a VING unit cell with account for surface traps.

The capacitance (C) of the test structure (VING or thin film) was determined by connecting a resistive load (R_L) in parallel to the structure and by analyzing the output potential pulse. When a mechanical compression was applied, a voltage pulse was generated, which decayed as a function of time, following a capacitive discharging process (see Figure S3, Supporting information). The calculation of the time constant τ of this process ($\tau^{-1} = R_L\,C$) allowed us to extract the capacitance. The piezoelectric coefficient d_{33}^{eff} for the piezoelectric structure was derived from voltage on top electrode (V_{top}), applied force (F), and capacitance using Eq. 9: [60]

$$d_{33}^{eff} = \frac{\mathrm{C}\,V_{top}(t_{0+})}{F(t_{0+})}\,, \tag{9}$$

where t_{0+} refers to the origin of time, immediately after mechanical loading by force F at t_0.

3.3. Mechanical and electrical boundary conditions

Figure 4 describes the mechanical and electrical boundary conditions used for a VING single cell and for a thin film. The thin film was used here as reference model and to validate our approach as will be detailed in the results section. Mechanical boundary conditions are specified in Fig. 4 (a). They consisted in i) a vertical pressure of -1 MPa along the NW axis (z-axis) on the top surface of the cell, being similarly applied to the thin film, with free vertical and lateral displacement (this corresponds to a locally applied force of about 126 nN), ii) free lateral displacement with forbidden vertical displacement on bottom side, iii) free lateral and vertical displacement on the lateral side and iv) free vertical displacement and forbidden lateral displacement on the axis of symmetry. In terms of electrical boundary conditions (Fig. 4(b)), the bottom electrode was grounded. The top surface was connected to the external resistive load by coupling equations 10 and 11 (Terminal definition under COMSOL).

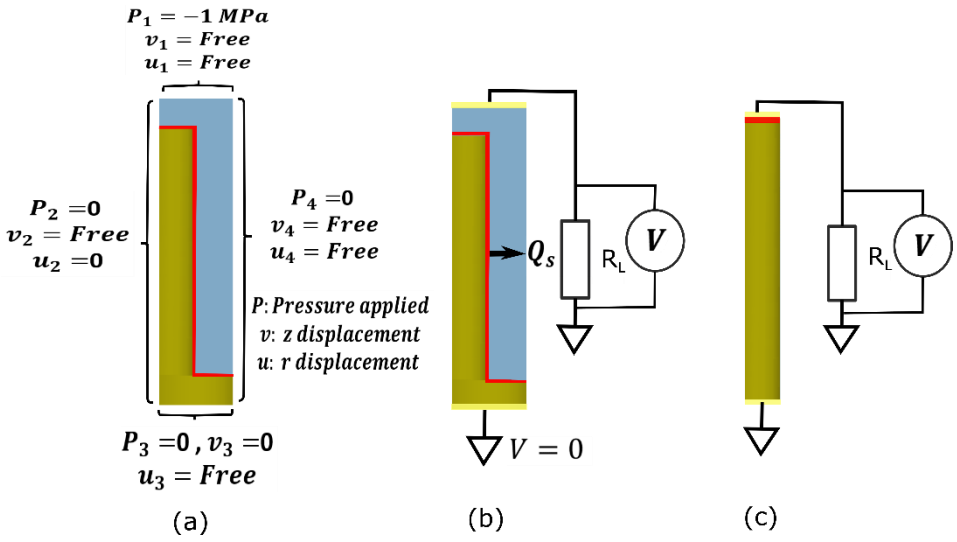

Fig. 4. Illustration of the VING single cell with (a) mechanical boundary conditions. Electrical boundary condition for (b) VING single cell and (c) a thin film cell. The red coloured interface represent the region where a surface charge (Q_s) is considered.

Equation 10 defines the electric charge at the top surface (Q_{top}) of the device. Equation 11 defines electric current (I) that flows through the resistance.

$$\iint_{\Omega} D(t) \cdot \hat{n} = Q_{top}(t) \tag{10}$$

$$I(t) = \frac{\partial Q_{top}(t)}{\partial t} \tag{11}$$

The difference with most presently published simulations is that we introduced a surface charge Q_s at the interface between ZnO and PMMA. This interface includes top and sides of the nanowire and top of the seed layer for the NG unit cell, and top surface only for the thin film. This surface charge density depends on the local electric potential. It introduces a discontinuity in the normal component of $\vec{D}$ at ZnO/PMMA interfaces:

$$\vec{n} \cdot \kappa \vec{\nabla} V(t) = Q_s(t) \ . \tag{10}$$

At thermal equilibrium and assuming a uniform traps density (N_{it}), Q_s was expressed as a function of local potential V as:

$$Q_s(t) = \ -q^2 \ N_{it} \ (V(t) - \varphi_{Fi}) \ , \tag{11}$$

where φ_{Fi} is the difference between Fermi level and intrinsic level. We will come back later on this boundary condition to explain how it was used to mimic ultra-slow and ultra-fast traps.
Finally, the results obtained under these assumptions were also compared with those obtained with a free SFL, where there is a continuity of the normal component of the electric displacement field at the interface between ZnO and PMMA.

The piezoresponse to the "Press" action was defined as the variation of the top electrode potential (voltage across the resistive load) when a pressure was applied on the cell. The system without pressure was called here #1 (with a corresponding top electrode potential V_{top1}(t)), while the system under applied pressure was called here #2 (with a corresponding top electrode potential V_{top2}(t)). The piezoresponse was defined as the peak value of V_{top2}(t)-V_{top1}(t). For reverse "Release" action, the piezoresponse was instead given by V_{top1}(t)-V_{top2}(t). It has been verified that this peak value was equal to the value found with static simulation. The advantage of using time-dependent simulation is that it further allows the evaluation of d_{33}^{eff}, as discussed later on.

3.3. Traps dynamics

As a first trial towards a full account for traps dynamics, we considered two limiting cases. The first one, corresponding to "ultra-fast traps" assumed that thermodynamic equilibrium was maintained at all time. Under this assumption, Q_s was calculated in a fully self-consistent manner as a function of potential for systems #1 and #2, Q_{s1} and Q_{s2} being functions of V_1 and V_2, respectively. The second case of "ultra-slow traps" assumed that, during the mechanical transient, Q_s remained frozen at the value it had in the initial state. For the simulation of the "Press" action, where the initial state corresponds to system#1 and the final state corresponds to system#2, we solved the system of equations corresponding to system#2, except for Q_s, which was set to its self-consistent value calculated for system#1 (as in ref. [20]). Conversely, for the simulation of the "Release" action, we solved the system of equations corresponding to system#1 with Q_s calculated for system#2.

4. Results and discussion

In this section, we will start by comparing the piezoresponse of two different structures (VING and thin film), and the possible differences between "Press" and "Release" actions as well as between "ultra-slow traps" and "ultra-fast traps" for a VING unit cell.

4.1 Comparison between a VING and a thin film

Fig. 5 (a) compares the piezoresponse values of VING and thin film structures under external pressure resulting from "Press" action and shows their variations as a function of trap density in the case of ultra-slow traps. At low N_{it} (between $1x\ 10^{11}\ eV^{-1}cm^{-2}$ and $4\ x\ 10^{11}\ eV^{-1}cm^{-2}$), the piezoresponse of both systems was small because of piezoelectric field screening by free charges in doped ZnO. In both cases, the depleted region builded up only at the top of ZnO [15-17, 20, 61]. By increasing N_{it}, the piezoresponse values increased for both VING and thin film. The VING structure provided a better piezoresponse (around 600 mV), which was 40 times larger than that of the thin-film structure (15 mV). This was explained by the increased extension of the depletion region (where screening is suppressed) at the interface between ZnO and PMMA, including along the lateral sides of the NW, thus allowing the full depletion of the whole NW

height, as already shown in ref. [20,53], while the depletion was confined to top surface in the case of a film.

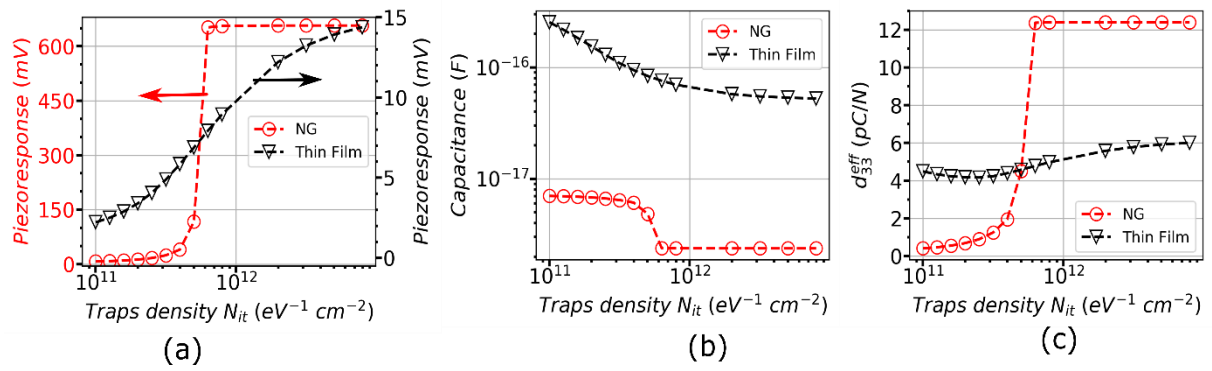

Fig. 5. (a) Maximum value of the piezoresponse at t=0 (b) capacitance and (c) effective piezoelectric coefficient as function of the ultra-slow trap density for two different structures: a VING single cell (⊙) and a thin film (∇) in "Press" action mode. A doping concentration $N_d = 10^{17}\ cm^{-3}$ was considered in the simulations.

By analyzing the voltage pulse (see an exemple of such a pulse in the Fig. S3 of Supporting Information) obtained for each system with different values of N_{it}, the capacitance value was extracted for both structures. Fig. 5(b) shows that the capacitance was larger by about one order of magnitude for the thin film than for the NG structure, and it decreased as N_{it} increases. This is a consequence of the extension of the depletion region which acts as an insulating region whose thickness increases as traps density increases. Eq. 9 was used to deduce d_{33}^{eff} from the results shown in Fig. 5 (a) and (b), with account for the force applied on the top surface (around 126 nN for 1 MPa compression). To verify our extraction method, two thin films were simulated: one semiconducting with free SFL (no traps, doping atoms, free carriers) and another one without semiconducting properties (no traps, no doping atoms, no free carriers, equivalent to a non-charged insulator). The calculated d_{33}^{eff} values were around 6 pC/N (Table S2 in Supporting Information and Fig. 5 (c) at high N_{it}), in fair agreement with the values expected for such thin film. Fig. 5 (c) shows that there is a dependency between d_{33}^{eff} and N_{it}. This dependence is stronger in the VING due to its high surface-to-volume ratio. Similarly to the piezoresponse trend, the maximum d_{33}^{eff} values were reached at high N_{it}.

These results are in good agreement with recent experimental findings for ZnO NWs [32, 36, 54–56] and ZnO thin films [38, 40–42] . In these reports, d_{33}^{eff} has been estimated to be in the range

of 2-15 pm/V (units equivalent to pC/N) for ZnO NWs, and between 2.5 to 8 pm/V for ZnO thin films.

Another remarkable conclusion of these simulations, detailed in the Supporting Information, was that an inverse piezoelectric effect can be observed at large N_{it} without any applied force on the top surface of VING. This inverse piezoelectric effect was strongly present on the top surface of ZnO NW as well as on the top of seed layer of ZnO material as N_{it} increases as shown in Figure S4. This added a piezoelectric polarization of the ZnO NW, with a z-component of opposite sign, compared to that resulting from vertical compression (details in Supporting Information, Fig. S5).

4.2 Symmetry and asymmetry of the piezoresponse to "Press" and "Release" actions

Fig. 6 was obtained in the case of ultra-slow traps. It shows that, when trap density is either low ($N_{it} \lesssim 0.4\text{x}10^{11}$ $eV^{-1}cm^{-2}$) or high ($N_{it} \gtrsim 1.1\text{x}10^{12}$ $eV^{-1}cm^{-2}$), the pizeoresponse, as well as the capacitance, are identical in "Press" and "Release" modes. This is expected. Indeed, for a very low trap density, independently of its exact value, free carriers almost complete screen the piezoelectric effect, so that the piezoresponse is negligible for both actions. On the other side, independently of its exact value, a high charge surface density results in a fully depleted NW, leading to the same response for both actuation modes.

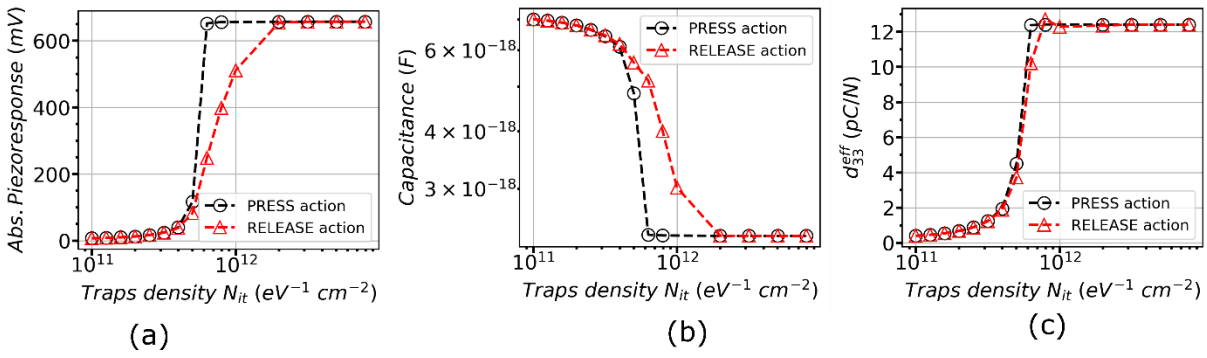

Fig. 6. Comparison between the "Press" and "Release" action modes as a function of trap density: (a) absolute value of the piezoresponse, (b) capacitance, and (c) on the piezoelectric coefficient of the unit cell. Curves obtained under the assumption of ultra-slow traps.

However, a different response was observed for intermediate of values of N_{it}, for which the different initial conditions combined with the assumption of ultra-slow traps lead to different results. This asymmetry is explained in more details in the Supporting Information (See Figures S6, S7 and S8), for $N_{it} = 10^{12}\ eV^{-1}cm^{-2}$. It is shown that the charge density of surface traps calculated without pressure (used for "Press" action) and with pressure (used for "Release" action) is sufficiently different to affect the distribution of free carriers and screening effects in these two action modes (Fig. 7). It is concluded that the presence of slow traps could explain the asymmetry of the piezoresponse observed in some experiments under compressive or bending actuation [11,20,62], while fast traps would favour symmetrical piezoresponse.

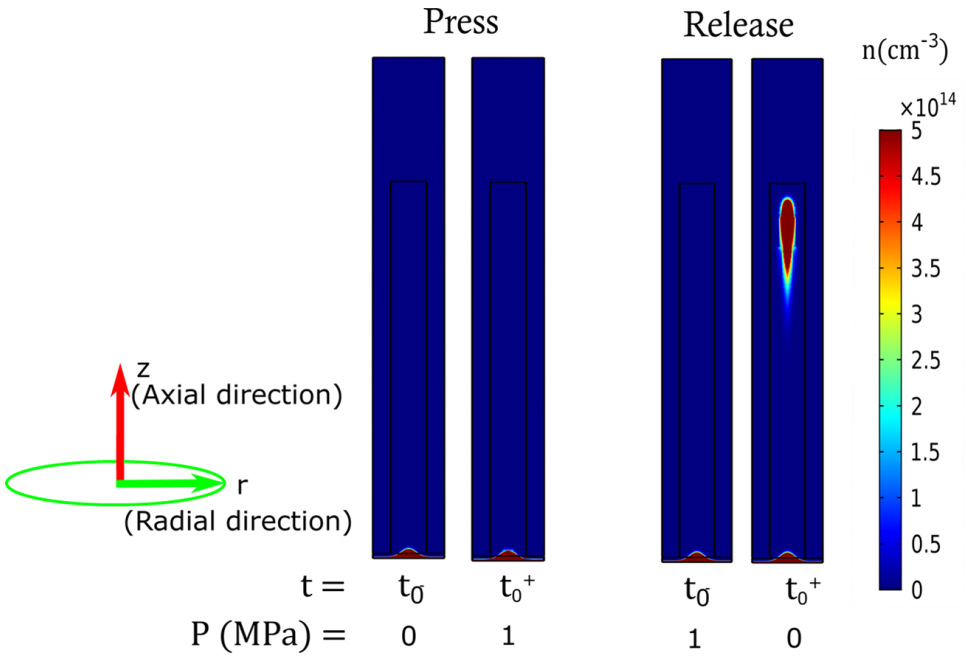

Fig. 7. Evolution of the free carrier distribution between t_{0^-} and t_{0^+} (just before and just after mechanical loading, respectively) for the "Press" and "Release" action. Compression 1 MPa along axial direction. Density of interface traps $N_{it} = 10^{12}\ eV^{-1}cm^{-2}$. Ultra-slow traps. After 'Release', a non negligible concentration of free carriers stays in the middle of the nanowire, while the nanowire is fully depleted otherwise. In contrast, the nanowire remains depleted during "Press" action.

The effective piezoelectric coefficient d_{33}^{eff} was calculated using Eq. (9) for both actuation modes as a function of interface traps density. Figure 6(c) shows that this coefficient was basically independent of the actuation mode ("Press" or "Release") but depended strongly on traps density.

From our simulations, we can expect that a medium-to-large density of traps will affect significantly the apparent piezoelectric properties of ZnO NWs and ZnO based nanocomposites. We believe that differences in interface properties could then explain the large dispersion of experimental values observed in the literature.

4.3 Towards an understanding of ultra-fast and ultra-slow traps influence

Another very important aspect to consider is the dynamics of surface traps. The ultra-slow traps considered above were assumed to reach thermodynamic equilibrium (TE) very slowly. As a consequence, traps charge did not vary during the application of the external mechanical load, and we could consider surface traps as frozen, with no participation to screening. This dynamics helped improving significantly the potential generation and the piezoelectric coefficient. On the other hand, ultra-fast traps reached TE instantly, thus contributing to the screening effect inside the NG, as shown in Figs. 8 (a) and 8 (b). With ultra-fast traps, both piezoresponse and d_{33}^{eff} tended to remain small or even decrease for a large range of trap density.

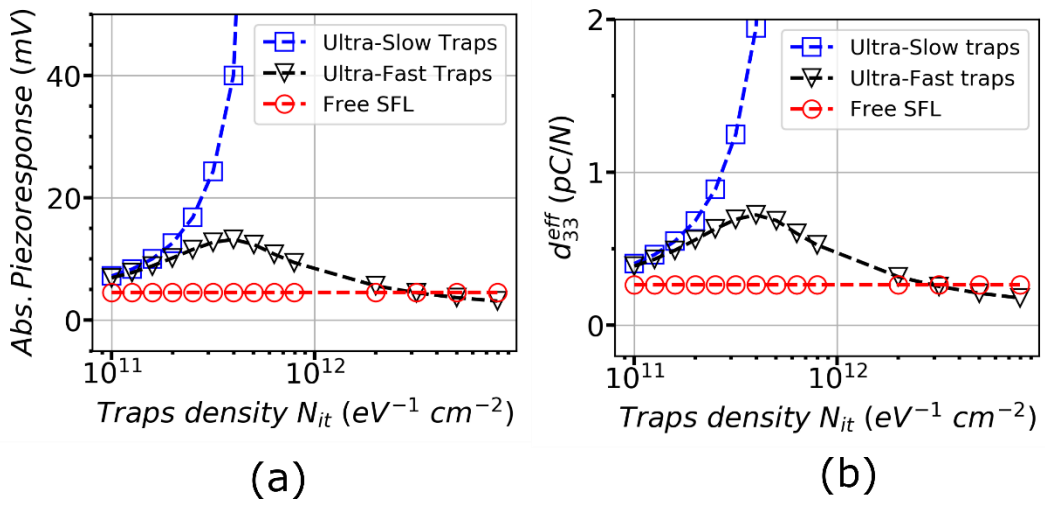

Fig. 8. (a) Variation of the piezoresponse in "Press" action mode. (b) Comparison of the d_{33}^{eff} piezoelectric coefficient as a function of trap density in "Press" action mode. These graphs compare results obtained with ultra-slow traps (⊡), ultra-fast traps (△) and free SFL (⊙).

To further analyse the impact of surface trap dynamics in ZnO NWs, we also reported in Fig. 8 (a) and Fig. 8 (b) the results obtained for a system without surface traps (i.e., free SFL), which are in

agreement with those illustrated in refs. [15,16,51] for similar geometry parameters, mechanical conditions and doping concentration N_d. The magnitude of the piezoresponse in these papers is very close to that observed for a large density of ultra-fast traps. However, as mentioned above, the large piezoresponse obtained with ultra-slow traps is in better agreement with experimental results [12,48].

Finally, there is presently an ongoing debate about the frequency dependence of d_{33}^{eff} values extracted from Piezoelectric Force Microscopy (PFM) measurements, which are based on the inverse piezoelectric effect, where an electric signal is applied to the sample. For example, some experimental works report values between 2.7 to 5 $pm\,V^{-1}$ in the range of 30-40 kHz [63,64], while others report a single value of 11.8 $pm\,V^{-1}$ in the range of 40 kHz-100 kHz [33]. These frequency ranges were chosen to reduce the contribution of electrostatic effects in the measurements. We speculate that a low-frequency signal could provide enough time to the system to maintain thermal equilibrium, which would better correspond to the case of ultra-fast traps, thus reducing the value of d_{33}^{eff}, as shown in Fig. 8 (b). In contrast, at higher frequencies, the traps may not have enough time to charge/discharge quickly, and would thus behave as ultra-slow traps (although in an intermediate state corresponding to the mean mechanical load), and d_{33}^{eff} may increase considerably. This would be consistent with the experimental trend and would provide a clear evidence of the important role of surface traps and of their dynamics in the study of piezoelectric phenomena in devices based on piezoelectric semiconducting nanostructures.

4. Conclusions

From this work, we can conclude that a certain amount of surface traps is required in order to obtain a piezoresponse of practical use from devices integrating ZnO NWs, for the range of dimensions and doping level reported in most experimental results. With a too low density of surface traps, most of the polarization field would be screened by free carriers. However, we found that the influence of surface traps was strongly dependent on their dynamics. Fast responding traps, which adapt immediately to the new thermodynamic equilibrium, partly screened the piezoelectric field generated by the external mechanical load. This screening was

especially efficient for large trap densities. In contrast, slow surface traps remaining filled at their initial level were unable to screen the changes in polarization induced by the application – or the release – of the external mechanical load. This allowed much larger piezoelectric responses to be reached. This also affected directly the effective piezoelectric coefficient of the structures (thin films and nanocomposites) and could explain the variability of the experimental values found in the literature. This study thus demonstrated that the realistic modelling of the piezoelectric response of semiconductor based sensors or energy harvesters should account for traps dynamics effects. For nanocomposite-based devices, experimental results about the quality of the interface between the semiconducting piezoelectric material and the insulating matrix would be of prime importance.

Acknowledgements: This work has been partly supported by the ANR projects SCENIC (under grant agreement ANR-20-CE09-0005) and LATINO (under grant agreement ANR-21-CE50-0026) from the French Ministry of Research and by the project PULSE-COM of the European Union's Horizon 2020 research and innovation programme under grant agreement No 863227.

References

[1] Q. Wan, Q.H. Li, Y.J. Chen, T.H. Wang, X.L. He, J.P. Li, C.L. Lin, Fabrication and ethanol sensing characteristics of ZnO nanowire gas sensors, Appl. Phys. Lett. 84 (2004) 3654–3656. https://doi.org/10.1063/1.1738932.

[2] B. Kumar, S.W. Kim, Energy harvesting based on semiconducting piezoelectric ZnO nanostructures, Nano Energy. 1 (2012) 342–355. https://doi.org/10.1016/j.nanoen.2012.02.001.

[3] Y. Zhang, Y. Liu, Z.L. Wang, Fundamental theory of piezotronics, Adv. Mater. 23 (2011) 3004–3013. https://doi.org/10.1002/adma.201100906.

[4] Q. Yang, X. Guo, W. Wang, Y. Zhang, S. Xu, D.H. Lien, Z.L. Wang, Enhancing Sensitivity of a Single ZnO Micro-/Nanowire Photodetector by Piezo-phototronic Effect, ACS Nano. 4 (2010) 6285–6291. https://doi.org/10.1021/nn1022878.

[5] O. Lupan, V.M. Guérin, I.M. Tiginyanu, V. V. Ursaki, L. Chow, H. Heinrich, T. Pauporté, Well-aligned arrays of vertically oriented ZnO nanowires electrodeposited on ITO-coated glass and their integration in dye sensitized solar cells, J. Photochem. Photobiol. A Chem. 211 (2010) 65–73. https://doi.org/10.1016/j.jphotochem.2010.02.004.

[6] Y. Zhang, H. Jia, R. Wang, C. Chen, X. Luo, D. Yu, C. Lee, Low-temperature growth and Raman scattering study of vertically aligned ZnO nanowires on Si substrate, Appl. Phys. Lett. 83 (2003) 4631–4633. https://doi.org/10.1063/1.1630849.

[7] M. Riaz, J. Song, O. Nur, Z.L. Wang, M. Willander, Study of the piezoelectric power generation of ZnO nanowire arrays grown by different methods, Adv. Funct. Mater. 21 (2011) 628–633. https://doi.org/10.1002/adfm.201001203.

[8] Z. Wang, X. Pan, Y. He, Y. Hu, H. Gu, Y. Wang, Piezoelectric Nanowires in Energy Harvesting Applications, Adv. Mater. Sci. Eng. 2015 (2015). https://doi.org/10.1155/2015/165631.

[9] Y. Zi, Z.L. Wang, Nanogenerators: An emerging technology towards nanoenergy, APL Mater. 5 (2017) 074103. https://doi.org/10.1063/1.4977208.

[10] A. Yu, H. Li, H. Tang, T. Liu, P. Jiang, Z.L. Wang, Vertically integrated nanogenerator based on ZnO nanowire arrays, Phys. Status Solidi - Rapid Res. Lett. 5 (2011) 162–164. https://doi.org/10.1002/pssr.201105120.

[11] R. Tao, M. Parmar, G. Ardila, P. Oliveira, D. Marques, L. Montès, M. Mouis, Performance of ZnO based piezo-generators under controlled compression, Semicond. Sci. Technol. 32 (2017) 064003. https://doi.org/10.1088/1361-6641/aa691f.

[12] Y. Hu, L. Lin, Y. Zhang, Z.L. Wang, Replacing a battery by a nanogenerator with 20 v output, Adv. Mater. 24 (2012) 110–114. https://doi.org/10.1002/adma.201103727.

[13] G. Zhu, A.C. Wang, Y. Liu, Y. Zhou, Z.L. Wang, Functional electrical stimulation by nanogenerator with 58 v output voltage, Nano Lett. 12 (2012) 3086–3090. https://doi.org/10.1021/nl300972f.

[14] C.H. Wang, W.S. Liao, Z.H. Lin, N.J. Ku, Y.C. Li, Y.C. Chen, Z.L. Wang, C.P. Liu, Optimization of the output efficiency of GaN nanowire piezoelectric nanogenerators by tuning the free carrier concentration, Adv. Energy Mater. 4 (2014) 1–7. https://doi.org/10.1002/aenm.201400392.

[15] R. Hinchet, S. Lee, G. Ardila, L. Montès, M. Mouis, Z.L. Wang, Performance optimization of vertical nanowire-based piezoelectric nanogenerators, Adv. Funct. Mater. 24 (2014) 971–977. https://doi.org/10.1002/adfm.201302157.

[16] G. Romano, G. Mantini, A. Di Carlo, A. D'Amico, C. Falconi, Z.L. Wang, Piezoelectric potential in vertically aligned nanowires for high output nanogenerators, Nanotechnology. 22 (2011) 465401. https://doi.org/10.1088/0957-4484/22/46/465401.

[17] S. Fathi, T.F. Sheikholeslami, Investigation of external charges effects on piezoelectric ZnO nanogenerator, J. Nano- Electron. Phys. 8 (2016) 6–11. https://doi.org/10.21272/jnep.8(2).02047.

[18] S. Min Kim, H. Kim, Y. Nam, S. Kim, Effects of external surface charges on the enhanced piezoelectric potential of ZnO and AlN nanowires and nanotubes, AIP Adv. 2 (2012) 042174. https://doi.org/10.1063/1.4770314.

[19] V.F. Rivera, F. Auras, P. Motto, S. Stassi, G. Canavese, E. Celasco, T. Bein, B. Onida, V. Cauda, Length-dependent charge generation from vertical arrays of high-aspect-ratio ZnO nanowires, Chem. - A Eur. J. 19 (2013) 14665–14674. https://doi.org/10.1002/chem.201204429.

[20] R. Tao, M. Mouis, G. Ardila, Unveiling the Influence of Surface Fermi Level Pinning on the Piezoelectric Response of Semiconducting Nanowires, Adv. Electron. Mater. 4 (2018) 1–9. https://doi.org/10.1002/aelm.201700299.

[21] J.P. Long, V.M. Bermudez, Band bending and photoemission-induced surface photovoltages on clean n- and p-GaN (0001) surfaces, Phys. Rev. B - Condens. Matter Mater. Phys. 66 (2002) 1213081–1213084. https://doi.org/10.1103/PhysRevB.66.121308.

[22] V. Portz, M. Schnedler, H. Eisele, R.E. Dunin-Borkowski, P. Ebert, Electron affinity and surface states of GaN m -plane facets: Implication for electronic self-passivation, Phys. Rev. B. 97 (2018) 1–5. https://doi.org/10.1103/PhysRevB.97.115433.

[23] A. Winnerl, R.N. Pereira, M. Stutzmann, Photo-induced changes of the surface band bending in GaN: Influence of growth technique, doping and polarity, J. Appl. Phys. 121 (2017). https://doi.org/10.1063/1.4983846.

[24] M. Landmann, E. Rauls, W.G. Schmidt, M.D. Neumann, E. Speiser, N. Esser, GaN m -plane: Atomic structure, surface bands, and optical response, Phys. Rev. B - Condens. Matter Mater. Phys. 91 (2015) 1–8. https://doi.org/10.1103/PhysRevB.91.035302.

[25] M.A. Reshchikov, M. Foussekis, A.A. Baski, Surface photovoltage in undoped n-type GaN, J. Appl. Phys. 107 (2010). https://doi.org/10.1063/1.3430979.

[26] Z.M. Liao, H.Z. Zhang, Y.B. Zhou, J. Xu, J.M. Zhang, D.P. Yu, Surface effects on photoluminescence of single ZnO nanowires, Phys. Lett. Sect. A Gen. At. Solid State Phys. 372 (2008) 4505–4509. https://doi.org/10.1016/j.physleta.2008.04.013.

[27] M.W. Allen, C.H. Swartz, T.H. Myers, T.D. Veal, C.F. McConville, S.M. Durbin, Bulk transport measurements in ZnO: The effect of surface electron layers, Phys. Rev. B - Condens. Matter Mater. Phys. 81 (2010) 1–6. https://doi.org/10.1103/PhysRevB.81.075211.

[28] W.A. Tisdale, M. Muntwiler, D.J. Norris, E.S. Aydil, X.-Y. Zhu, Electron Dynamics at the ZnO $(10\bar{1}0)$ Surface, J. Phys. Chem. C. 112 (2008) 14682–14692. https://doi.org/10.1021/jp802455p.

[29] R. Heinhold, G.T. Williams, S.P. Cooil, D.A. Evans, M.W. Allen, Influence of polarity and hydroxyl termination on the band bending at ZnO surfaces, Phys. Rev. B - Condens. Matter Mater. Phys. 88 (2013) 38–40. https://doi.org/10.1103/PhysRevB.88.235315.

[30] A. Soudi, C.-H. Hsu, Y. Gu, Diameter-Dependent Surface Photovoltage and Surface State Density in Single Semiconductor Nanowires, Nano Lett. 12 (2012) 5111–5116. https://doi.org/10.1021/nl301863e.

[31] M.J. Al-Saadi, S.H. Al-Harthi, H.H. Kyaw, M.T.Z. Myint, T. Bora, K. Laxman, A. Al-Hinai, J. Dutta, Influence of Atomic Hydrogen, Band Bending, and Defects in the Top Few Nanometers of Hydrothermally Prepared Zinc Oxide Nanorods, Nanoscale Res. Lett. 12 (2017) 22. https://doi.org/10.1186/s11671-016-1800-3.

[32] C. Zhang, X. Wang, W. Chen, J. Yang, An analysis of the extension of a ZnO piezoelectric semiconductor nanofiber under an axial force, Smart Mater. Struct. 26 (2017). https://doi.org/10.1088/1361-665X/aa542e.

[33] D. Tamvakos, S. Lepadatu, V.A. Antohe, A. Tamvakos, P.M. Weaver, L. Piraux, M.G. Cain, D. Pullini, Piezoelectric properties of template-free electrochemically grown ZnO nanorod arrays, Appl. Surf. Sci. 356 (2015) 1214–1220. https://doi.org/10.1016/j.apsusc.2015.08.187.

[34] E. Broitman, M.Y. Soomro, J. Lu, M. Willander, L. Hultman, Nanoscale piezoelectric response of ZnO nanowires measured using a nanoindentation technique, Phys. Chem. Chem. Phys. 15 (2013) 11113. https://doi.org/10.1039/c3cp50915j.

[35] H.J. Fan, W. Lee, R. Hauschild, M. Alexe, G. Le Rhun, R. Scholz, A. Dadgar, K. Nielsch, H. Kalt, A. Krost, M. Zacharias, U. Gösele, Template-Assisted Large-Scale Ordered Arrays of ZnO Pillars for Optical and Piezoelectric Applications, Small. 2 (2006) 561–568. https://doi.org/10.1002/smll.200500331.

[36] D.A. Scrymgeour, T.L. Sounart, N.C. Simmons, J.W.P. Hsu, Polarity and piezoelectric response of solution grown zinc oxide nanocrystals on silver, J. Appl. Phys. 101 (2007) 014316. https://doi.org/10.1063/1.2405014.

[37] D. Cavallini, M. Fortunato, G. De Bellis, M.S. Sarto, PFM Characterization of Piezoelectric PVDF/ZnO-N Anorod Thin Films, Proc. IEEE Conf. Nanotechnol. 2018-July (2019) 1–3. https://doi.org/10.1109/NANO.2018.8626362.

[38] Q.C. Bui, G. Ardila, E. Sarigiannidou, H. Roussel, C. Jiménez, O. Chaix-Pluchery, Y. Guerfi, F. Bassani, F. Donatini, X. Mescot, B. Salem, V. Consonni, Morphology Transition of ZnO from Thin Film to Nanowires on Silicon and its Correlated Enhanced Zinc Polarity Uniformity and Piezoelectric Responses, ACS Appl. Mater. Interfaces. 12 (2020) 29583–29593. https://doi.org/10.1021/acsami.0c04112.

[39] M.-H. Zhao, Z.-L. Wang, S.X. Mao, Piezoelectric Characterization of Individual Zinc Oxide Nanobelt Probed by Piezoresponse Force Microscope, Nano Lett. 4 (2004) 587–590. https://doi.org/10.1021/nl035198a.

[40] M. Laurenti, S. Stassi, M. Lorenzoni, M. Fontana, G. Canavese, V. Cauda, C.F. Pirri, Evaluation of the piezoelectric properties and voltage generation of flexible zinc oxide thin films, Nanotechnology. 26 (2015) 215704. https://doi.org/10.1088/0957-4484/26/21/215704.

[41] K. Zhang, Y. Zhao, F. He, D. Liu, Piezoelectricity of ZnO Films Prepared by Sol-Gel Method, Chinese J. Chem. Phys. 20 (2007) 721–726. https://doi.org/10.1088/1674-0068/20/06/721-726.

[42] P. Sharma, Z. Guler, N. Jackson, Development and characterization of confocal sputtered piezoelectric zinc oxide thin film, Vacuum. 184 (2021) 109930. https://doi.org/10.1016/j.vacuum.2020.109930.

[43] S. Kim, D. Seol, X. Lu, M. Alexe, Y. Kim, Electrostatic-free piezoresponse force microscopy, Sci. Rep. 7 (2017) 41657. https://doi.org/10.1038/srep41657.

[44] L. Jaloustre, S. Le Denmat, T. Auzelle, M. Azadmand, L. Geelhaar, F. Dahlem, R. Songmuang, Toward Quantitative Measurements of Piezoelectricity in III-N Semiconductor Nanowires, ACS Appl. Nano Mater. 4 (2021) 43–52. https://doi.org/10.1021/acsanm.0c02078.

[45] N. Novak, P. Keil, T. Frömling, F.H. Schader, A. Martin, K.G. Webber, J. Rödel, Influence of metal/semiconductor interface on attainable piezoelectric and energy harvesting properties of ZnO, Acta Mater. 162 (2019) 277–283. https://doi.org/10.1016/j.actamat.2018.10.008.

[46] S.M. Kim, J.I. Sohn, H.J. Kim, J. Ku, Y.J. Park, S.N. Cha, J.M. Kim, Radially dependent effective piezoelectric coefficient and enhanced piezoelectric potential due to geometrical stress confinement in ZnO nanowires/nanotubes, Appl. Phys. Lett. 101 (2012) 013104. https://doi.org/10.1063/1.4731779.

[47] M.-T. Hoang, J. Yvonnet, A. Mitrushchenkov, G. Chambaud, First-principles based multiscale model of piezoelectric nanowires with surface effects, J. Appl. Phys. 113 (2013) 014309. https://doi.org/10.1063/1.4773333.

[48] S. Xu, Y. Qin, C. Xu, Y. Wei, R. Yang, Z.L. Wang, Self-powered nanowire devices, Nat. Nanotechnol. 5 (2010) 366–373. https://doi.org/10.1038/nnano.2010.46.

[49] Y. Gao, Z.L. Wang, Equilibrium potential of free charge carriers in a bent piezoelectric semiconductive nanowire, Nano Lett. 9 (2009) 1103–1110. https://doi.org/10.1021/nl803547f.

[50] S. Min Kim, H. Kim, Y. Nam, S. Kim, Effects of external surface charges on the enhanced piezoelectric potential of ZnO and AlN nanowires and nanotubes, AIP Adv. 2 (2012). https://doi.org/10.1063/1.4770314.

[51] R. Araneo, G. Lovat, P. Burghignoli, C. Falconi, Piezo-Semiconductive Quasi-1D Nanodevices with or without Anti-Symmetry, Adv. Mater. 24 (2012) 4719–4724. https://doi.org/10.1002/adma.201104588.

[52] J.I. Sohn, S.N. Cha, B.G. Song, S. Lee, S.M. Kim, J. Ku, H.J. Kim, Y.J. Park, B.L. Choi, Z.L. Wang, J.M. Kim, K. Kim, Engineering of efficiency limiting free carriers and an interfacial energy barrier for an enhancing piezoelectric generation, Energy Environ. Sci. 6 (2013) 97–104. https://doi.org/10.1039/c2ee23404a.

[53] A.J.L. Garcia, M. Mouis, V. Consonni, G. Ardila, Dimensional Roadmap for Maximizing the Piezoelectrical Response of ZnO Nanowire-Based Transducers: Impact of Growth Method, Nanomaterials. 11 (2021) 941. https://doi.org/https://doi.org/10.3390/nano11040941.

[54] R. Hinchet, S. Lee, G. Ardila, L. Montes, M. Mouis, Z.L. Wang, Design and guideline rules for the performance improvement of vertically integrated nanogenerator, J. Energy Power Eng. 7 (2013) 1816.

[55] N. Doumit, G. Poulin-Vittrant, A New Simulation Approach for Performance Prediction of Vertically Integrated Nanogenerators, Adv. Theory Simulations. 1 (2018) 1800033. https://doi.org/10.1002/adts.201800033.

[56] R. Tao, G. Ardila, L. Montès, M. Mouis, Modeling of semiconducting piezoelectric nanowires for mechanical energy harvesting and mechanical sensing, Nano Energy. 14 (2014) 62–76. https://doi.org/10.1016/j.nanoen.2014.11.035.

[57] A.S. Dahiya, F. Morini, S. Boubenia, K. Nadaud, D. Alquier, G. Poulin-Vittrant, Organic/Inorganic Hybrid Stretchable Piezoelectric Nanogenerators for Self-Powered Wearable Electronics, Adv. Mater. Technol. 3 (2018) 1700249. https://doi.org/10.1002/admt.201700249.

[58] G. Zhu, R. Yang, S. Wang, Z.L. Wang, Flexible high-output nanogenerator based on lateral ZnO nanowire array, Nano Lett. 10 (2010) 3151–3155. https://doi.org/10.1021/nl101973h.

[59] Y.B. Jeon, R. Sood, J.H. Jeong, S.G. Kim, MEMS power generator with transverse mode thin film PZT, Sensors Actuators, A Phys. 122 (2005) 16–22. https://doi.org/10.1016/j.sna.2004.12.032.

[60] A.J. Lopez Garcia, R. Tao, M. Mouis, G. Ardila, A New Approach to Calculate the Piezoelectric Coefficient of Piezo-Semiconductor Nanowires Integrated in Nanocomposites: Experiment and Simulation, in: 2021 21st Int. Conf. Solid-State Sensors, Actuators Microsystems, IEEE, 2021: pp. 1056–1059. https://doi.org/10.1109/Transducers50396.2021.9495621.

[61] G. Mantini, Y. Gao, A. D'Amico, C. Falconi, Z.L. Wang, Equilibrium piezoelectric potential distribution in a deformed ZnO nanowire, Nano Res. 2 (2009) 624–629. https://doi.org/10.1007/s12274-009-9063-2.

[62] R.S. Kammel, R.S. Sabry, Effects of the aspect ratio of ZnO nanorods on the performance of piezoelectric nanogenerators, J. Sci. Adv. Mater. Devices. 4 (2019) 420–424. https://doi.org/10.1016/j.jsamd.2019.08.002.

[63] K. Momeni, A. Asthana, A. Prasad, Y.K. Yap, R. Shahbazian-Yassar, Structural inhomogeneity and piezoelectric enhancement in ZnO nanobelts, Appl. Phys. A Mater. Sci. Process. 109 (2012) 95–100. https://doi.org/10.1007/s00339-012-7081-5.

[64] M.-H. Zhao, Z.-L. Wang, S.X. Mao, Piezoelectric Characterization of Individual Zinc Oxide Nanobelt Probed by Piezoresponse Force Microscope, Nano Lett. 4 (2004) 587–590. https://doi.org/10.1021/nl035198a.